

LDC-MTL: Balancing Multi-Task Learning through Scalable Loss Discrepancy Control

Peiyao Xiao* Chaosheng Dong[†] Shaofeng Zou[‡] Kaiyi Ji^{*§}

May 21, 2025

Abstract

Multi-task learning (MTL) has been widely adopted for its ability to simultaneously learn multiple tasks. While existing gradient manipulation methods often yield more balanced solutions than simple scalarization-based approaches, they typically incur a significant computational overhead of $\mathcal{O}(K)$ in both time and memory, where K is the number of tasks. In this paper, we propose LDC-MTL, a simple and scalable loss discrepancy control approach for MTL, formulated from a bilevel optimization perspective. Our method incorporates three key components: (i) a coarse loss pre-normalization, (ii) a bilevel formulation for fine-grained loss discrepancy control, and (iii) a scalable first-order bilevel algorithm that requires only $\mathcal{O}(1)$ time and memory. Theoretically, we prove that LDC-MTL guarantees convergence not only to a stationary point of the bilevel problem with loss discrepancy control but also to an ϵ -accurate Pareto stationary point for all K loss functions under mild conditions. Extensive experiments on diverse multi-task datasets demonstrate the superior performance of LDC-MTL in both accuracy and efficiency. Code is available at <https://github.com/OptMN-Lab/LDC-MTL>.

1 Introduction

In recent years, Multi-Task Learning (MTL) has received increasing attention for its ability to predict multiple tasks simultaneously using a single model, thereby reducing computational overhead. This versatility has enabled a wide range of applications, including autonomous driving (Chen et al., 2018), recommendation systems (Wang et al., 2020), and natural language processing (Zhang et al., 2022).

One of the main challenges in MTL is the imbalance and discrepancy in task losses, where different tasks progress at uneven rates during training. This discrepancy stems from several sources: variations in loss magnitudes due to differing units or scales (e.g., meters vs. millimeters) (Kendall et al., 2018; Liu et al., 2019), heterogeneity in task types (e.g., regression vs. classification) (Dai et al., 2023; Lin et al., 2021), and conflicting gradient directions across tasks (Yu et al., 2020; Liu et al., 2021a). When unaddressed, such discrepancies may cause certain tasks to dominate the optimization trajectory, ultimately leading to degraded performance on others.

*Peiyao Xiao and Kaiyi Ji are with the Department of Computer Science and Engineering, University at Buffalo, Buffalo, NY 14228 USA (e-mail: peiyaoxi@buffalo.edu, kaiyiji@buffalo.edu).

[†]Chaosheng Dong is with Amazon.com Inc, Seattle, WA, 98109 USA (e-mail: chaosd@amazon.com).

[‡]Shaofeng Zou is with the School of Electrical, Computer and Energy Engineering, Arizona State University, Tempe, AZ 85281 USA (e-mail: zou@asu.edu).

[§]Correspondence to: Kaiyi Ji (kaiyiji@buffalo.edu)

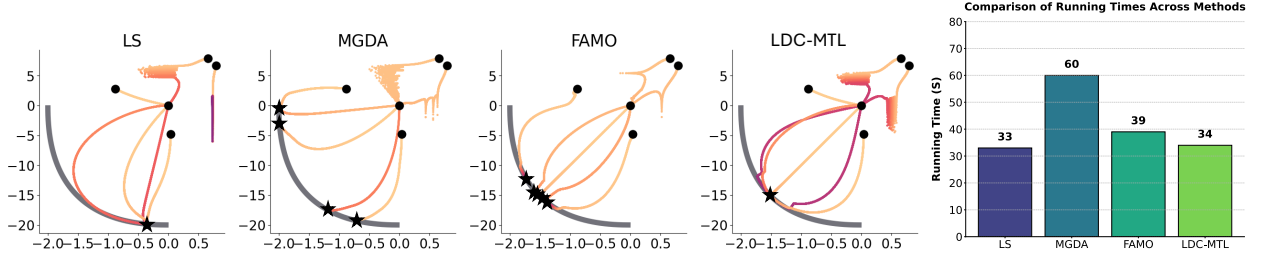


Figure 1: The loss trajectories of a toy 2-task learning problem from Liu et al. 2024 and the runtime comparison of different MTL methods for 50000 steps. Stars on the Pareto front denote the convergence points. Although FAMO (Liu et al., 2024) achieves more balanced results than Linear Scalarization (LS) and MGDA (Désidéri, 2012), it converges to different points on the Pareto front. LDC-MTL reaches the same balanced point with a computational cost comparable to the LS. Full experimental details can be found in Appendix A.3.

To mitigate this issue, MTL research generally follows two main paradigms. The first is the class of scalarization-based methods, which transform MTL into a single-objective optimization problem by aggregating task losses, typically through weighted or averaged sums. Early works adopted static weighting schemes for their simplicity and scalability (Caruana, 1997), but these often led to degraded multi-task performance relative to single-task baselines, largely due to persistent gradient conflicts under fixed weights (Xiao et al., 2024). As a remedy, more recent approaches explore dynamic loss weighting strategies that adapt during training (Kendall et al., 2018; Liu et al., 2019; Lin et al., 2021; Dai et al., 2023). However, these methods do not explicitly address loss discrepancy, allowing task interference to persist and leading to imbalanced performance across tasks. The second line of work involves gradient manipulation techniques, which aim to promote balanced optimization by explicitly resolving gradient conflicts. These approaches seek update directions that are more equitable across tasks (Désidéri, 2012; Liu et al., 2021a; Ban & Ji, 2024; Navon et al., 2022; Yu et al., 2020; Fernando et al., 2023; Xiao et al., 2024). While often effective in reducing task interference, they typically require computing and storing gradients from all K tasks at each iteration, incurring $O(K)$ time and memory costs. This scalability bottleneck poses challenges for large-scale MTL scenarios involving deep architectures and massive datasets.

In this paper, we propose a simple and scalable loss discrepancy control approach for MTL from a novel bilevel optimization perspective. Our approach comprises three key components: a coarse loss pre-normalization, a bilevel formulation for fine-grained loss discrepancy control, and a scalable first-order bilevel algorithmic design. Our specific contributions are summarized as follows.

- **Bilevel formulation for loss discrepancy control.** At the core of our bilevel formulation, the lower-level problem optimizes the model parameters by minimizing a weighted sum of normalized individual loss functions. Meanwhile, the upper-level problem adjusts these weights to minimize the discrepancies among the loss functions, ensuring balanced learning across tasks.
- **Scalable algorithms with only $O(1)$ time and memory cost.** We develop Loss Discrepancy Control for Multi-Task Learning (LDC-MTL), a highly efficient algorithm tailored to solve the proposed bilevel problem with loss discrepancy control. Unlike traditional bilevel methods, LDC-MTL has a fully single-loop structure without any second-order gradient computation, resulting in an overall $O(1)$ time and memory complexity. The 2-task toy example in Figure 1 illustrates that our LDC-MTL method achieves a more balanced solution compared to other competitive approaches while maintaining superior computational efficiency.

- **Superior empirical performance.** Extensive experiments demonstrate that our proposed LDC-MTL method achieves state-of-the-art performance compared to various scalarization-based and gradient manipulation methods across multiple supervised multi-task datasets, including QM9 (Ramakrishnan et al., 2014), CelebA (Liu et al., 2015), and Cityscapes (Cordts et al., 2016). Moreover, LDC-MTL stands out as one of the most efficient and scalable methods.
- **Comprehensive experimental analysis.** We conduct a comprehensive evaluation showing that task losses under LDC-MTL become more concentrated and consistently lower. As a beneficial side effect of controlling loss discrepancies, gradient conflicts are also alleviated. Moreover, we benchmark our method against weight-swept linear scalarization (LS) and find that LDC-MTL solutions lie on the Pareto frontier (PF) with consistently better results. Notably, our empirical results indicate that the dynamic training trajectory rather than the final model parameters, is key to achieving strong performance by our method. These findings collectively highlight the significance of dynamic loss discrepancy control in our approach.
- **Theoretical guarantees.** Theoretically, we show that LDC-MTL guarantees convergence not only to a stationary point of the bilevel problem with loss discrepancy control but also to an ϵ -accurate Pareto stationary point for all K individual loss functions.

2 Related Works

Multi-task learning. MTL has recently garnered significant attention in practical applications. One line of research focuses on model architecture, specifically designing various sharing mechanisms (Kokkinos, 2017; Ruder et al., 2019). Another direction addresses the mismatch in loss magnitudes across tasks, proposing methods to balance them. For example, Kendall et al. 2018 balanced tasks by weighting loss functions based on homoscedastic uncertainties, while Liu et al. 2019 dynamically adjusted weights by considering the rate of change in loss values for each task.

Besides, one prominent approach frames MTL as a Multi-Objective Optimization (MOO) problem. Sener & Koltun 2018 introduced this perspective in deep learning, inspiring methods based on the Multi-Gradient Descent Algorithm (MGDA) (Désidéri, 2012). Subsequent work has aimed to address gradient conflicts. For instance, PCGrad (Yu et al., 2020) resolves conflicts by projecting gradients onto the normal plane, GradDrop (Chen et al., 2020) randomly drops conflicting gradients, and CAGrad (Liu et al., 2021a) constrains update directions to balance gradients. Additionally, Nash-MTL (Navon et al., 2022) formulates MTL as a bargaining game among tasks, while FairGrad (Ban & Ji, 2024) incorporates α -fairness into gradient adjustments. Achituve et al. 2024 introduces a novel gradient aggregation approach using Bayesian inference to reduce the running time.

Prior works Kurin et al. 2022; Xin et al. 2022 have shown that several gradient-based MTL methods fail to consistently outperform linear scalarization (LS) with weight sweeping. In contrast, our extensive experiments, such as the scatter plot comparison, demonstrate that our method yields solutions that dominate those obtained by weight-swept LS. On the theoretical side, Zhou et al. 2022 analyzed the convergence properties of stochastic MGDA, and Fernando et al. 2023 proposed a method to reduce bias in the stochastic MGDA with theoretical guarantees. More recent advancements include a double-sampling strategy with provable guarantees introduced by Xiao et al. 2024 and Chen et al. 2024.

Bilevel optimization. Bilevel optimization, first introduced by Bracken & McGill 1973, has been extensively studied over the past few decades. Early research primarily treated it as a constrained optimization problem (Hansen et al., 1992; Shi et al., 2005). More recently, gradient-based methods have gained prominence due to their effectiveness in machine learning applications. Many of these approaches approximate

the hypergradient using either linear systems (Domke, 2012; Ji et al., 2021) or automatic differentiation techniques (Maclaurin et al., 2015; Franceschi et al., 2017). However, these methods become impractical in large-scale settings due to their significant computational cost (Xiao & Ji, 2023; Yang et al., 2024b). The primary challenge lies in the high cost of gradient computation: approximating the Hessian-inverse vector requires multiple first- and second-order gradient evaluations, and the nested sub-loops exacerbate this inefficiency. To address these limitations, recent studies have focused on reducing the computational burden of second-order gradients. For example, some methods reformulate the lower-level problem using value-function-based constraints and solve the corresponding Lagrangian formulation (Kwon et al., 2023; Yang et al., 2024a). The work studies convex bilevel problems and proposes a zeroth-order optimization method with finite-time convergence to the Goldstein stationary point (Chen et al., 2023). In this work, we propose a simplified first-order bilevel method for MTL, motivated by intriguing empirical findings.

3 Preliminary

Scalarization-based methods. MTL aims to optimize multiple tasks (objectives) simultaneously with a single model. The straightforward approach is to optimize a weighted summation of all loss functions: $\min_x L_{total}(x) = \sum_{i=1}^K w_i l_i(x)$, where $x \in \mathbb{R}^d$ denotes the model parameter, $l_i(x) : \mathbb{R}^d \rightarrow \mathbb{R}_{\geq 0}$ represents the loss function of the i -th task and K is the number of tasks. This approach faces three key challenges: 1) loss values could differ in scale 2) fixed weights can lead to significant gradient conflicts, potentially allowing one task to dominate the learning process (Xiao et al., 2024; Wang et al., 2024); and 3) the overall performance is highly sensitive to the weighting of different losses (Kendall et al., 2018). Consequently, such methods often struggle with performance imbalances across tasks.

Gradient manipulation methods. To mitigate gradient conflicts, gradient manipulation methods dynamically compute an update d^t at each epoch to balance progress across tasks, where t is the epoch index. The update d^t is typically a convex combination of task gradients, expressed as:

$$d^t = G(x^t)w^t, \text{ where } w^t = h(G(x^t)),$$

with $G(x^t) = [\nabla l_1(x^t), \nabla l_2(x^t), \dots, \nabla l_K(x^t)]^\top$. The weight vector w^t is determined by a function $h(\cdot) : \mathbb{R}^{K \times d} \rightarrow \mathbb{R}^K$, which varies depending on the specific method. However, these methods often require computing and storing the gradients of all K tasks during each epoch, making them less scalable and resource-intensive, particularly in large-scale scenarios. Therefore, it is necessary to develop lightweight methods that achieve balanced performance.

Pareto concepts. Solving the MTL problem is challenging because it is difficult to identify a common x that achieves the optima for all tasks. Instead, a widely accepted target is finding a Pareto stationary point. Suppose we have two points x_1 and x_2 . It is claimed that x_1 dominates x_2 if $l_i(x_1) \leq l_i(x_2) \forall i \in [K]$, and $\exists j \ l_j(x_1) < l_j(x_2)$. A point is Pareto optimal if it is not dominated by any other points, implying that no task can be improved further without sacrificing another. Besides, a point x is a Pareto stationary point if $\min_{w \in \mathcal{W}} \|G(x)w\| = 0$.

4 Loss Discrepancy Control for Multi-Task Learning

In this section, we present our bilevel loss discrepancy control framework for multi-task learning. As illustrated in Figure 2, this framework contains a coarse loss pre-normalization module, a fine-grained bilevel loss discrepancy control procedure, and a simplified first-order optimization design.

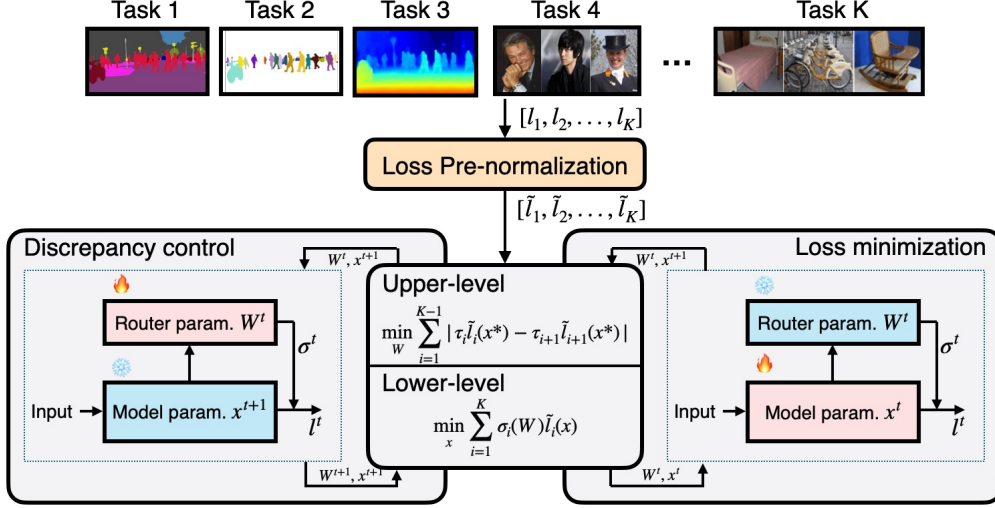


Figure 2: Our bilevel loss discrepancy control pipeline for multi-task learning. First, task losses will be normalized through a coarse loss pre-normalization module. Then, the lower-level problem optimizes the model parameter x^t by minimizing the weighted sum of task losses, and the upper-level problem optimizes the router model parameter W^t for fine-grained loss discrepancy control.

4.1 Loss pre-normalization

Before applying loss discrepancy control, a coarse loss pre-normalization step is introduced to ensure that the rescaled loss functions are on a similar and comparable scale. This step is necessary because training often involves tasks of different types (e.g., classification and regression) with distinct loss functions, as well as targets measured in varying units or scales (e.g., meters, centimeters, or millimeters). Here, we present two effective approaches that work well in different scenarios.

Rescaled normalization. This method normalizes loss values by rescaling each task’s loss using its initial loss value l'_i , such that $\tilde{l}_i = \frac{l_i}{l'_i}$. The resulting normalized loss reflects the training progress and ensures comparability across tasks. This approach is particularly well-suited for scenarios where the loss scales do not differ significantly.

Logarithmic normalization. In some cases, the loss can vary significantly in scale. For example, as shown in Figure 6 in the appendix, we observed that the loss values during training across 11 regression tasks in the QM9 dataset exhibit substantial differences in magnitude, with loss ratios exceeding 1000 in certain instances. To address this issue, we propose logarithmically rescaling the loss functions such that $\tilde{l}_i = \log\left(\frac{l_i}{l_{i,0}}\right)$, where $l_{i,0}$ represents the initial loss value for the i -th task at each epoch. Our experiments demonstrate that this initialization approach stabilizes training by reducing large fluctuations caused by significant scale variations.

4.2 Bilevel formulation for loss discrepancy control

Building on the normalized loss function values, we introduce a novel bilevel loss discrepancy control approach for MTL to achieve a more balanced and fair solution. The formulation is as follows:

$$\begin{aligned} \min_W \sum_{i=1}^{K-1} |\tau_i \tilde{l}_i(x^*) - \tau_{i+1} \tilde{l}_{i+1}(x^*)| &:= f(W, x^*) \\ \text{s.t. } x^* \in \arg \min_x \sum_{i=1}^K \sigma_i(W) \tilde{l}_i(x) &:= g(W, x), \end{aligned} \quad (1)$$

where we denote $x^* = x^*(W)$ for notational convenience. Note that we define a routing function $\sigma(W) \in \mathbb{R}^K$, which is parameterized by a small neural network with a softmax output layer. It takes the shared characteristic as the input and the output weights K for different tasks. For the upper-level weight vector $\tau = (\tau_1, \dots, \tau_K)$, we provide two effective options: (i) $\tau = \sigma(W)$ and (ii) $\tau = \mathbf{1}$ that work well in experiments. It can be seen from eq. (1) that the lower-level problem minimizes the weighted sum of losses w.r.t. the model parameters x , while the upper-level problem minimizes the accumulated weighted loss gaps w.r.t. the parameters W , controlling the loss discrepancy among tasks. Notably, the optimal solution does not require all losses to be equal, and there will be a trade-off between loss minimization and loss discrepancy control, as shown in Remark 1.

4.3 Scalable first-order algorithm design

To enable large-scale applications, we adopt an efficient first-order method to solve the problem in Equation (1). Inspired by recent advances in first-order bilevel optimization (Kwon et al., 2023; Yang et al., 2023), we reformulate the original bilevel problem into an equivalent constrained optimization problem as follows.

$$\min_W f(W, x) \quad \text{s.t.} \quad \underbrace{\sum_{i=1}^K \sigma_i(W) \tilde{l}_i(x) - \sum_{i=1}^K \sigma_i(W) \tilde{l}_i(x^*)}_{\text{penalty function } p(W, x)} \leq 0.$$

Then, given a penalty constant $\lambda > 0$, penalizing $p(W, x)$ into the upper-level loss function yields

$$\min_{W, x} f(W, x) + \lambda \sum_{i=1}^K \left(\sigma_i(W) \tilde{l}_i(x) - \sigma_i(W) \tilde{l}_i(x^*) \right). \quad (2)$$

Intuitively, a larger λ allows more precise training on model parameters x such that x converges closer to x^* . Conversely, a smaller λ prioritizes upper-level loss discrepancy control during training. The main challenge of solving the penalized problem above lies in the updates of W , as shown below:

$$W^{t+1} = W^t - \alpha \left(\nabla_W f(W^t, x^t) + \lambda (\nabla_W g(W^t, x^t) - \nabla_W g(W^t, z_N^t)) \right), \quad (3)$$

where t is the epoch index, α is the step size, and z_N^t is an approximation of $x_t^* \in \arg \min_x g(W^t, x)$ through the following loop of N iterations each epoch.

$$z_{n+1}^t = z_n^t - \beta \nabla_z g(W^t, z_n^t), n = 0, 1, \dots, N-1, \quad (4)$$

where N is typically chosen to be sufficiently large, ensuring that z_N^t closely approximates x_t^* (the full algorithm is provided in Algorithm 2 in the appendix). Consequently, this sub-loop of iterations incurs significant computational overhead, driven by the high dimensionality of z (matching that of the model parameters) and the large value of N .

Algorithm 1: LDC-MTL

```

Initialize:  $W^0, x^0$ 
for  $t = 0, 1, \dots, T-1$  do
     $x^{t+1} = x^t - \alpha (\nabla_x f(W^t, x^t) + \lambda \nabla_x g(W^t, x^t))$ 
     $W^{t+1} = W^t - \alpha (\nabla_W f(W^t, x^t) + \lambda \nabla_W g(W^t, x^t))$ 
end for

```

Remark 1. *This formulation encourages task losses to be close but not necessarily equal. The penalty constant λ controls the trade-off between minimizing the sum of weighted losses and reducing the loss discrepancy among tasks.*

Practical implementation. Our experiments show that the gradient norm $\|\nabla_W g(W^t, z_N^t)\|$ remains small, typically orders of magnitude smaller than the gradient norm $\|\nabla_W g(W^t, x^t)\|$, which is used to update the outer parameters W . This behavior is illustrated in Figure 7 in the Appendix. Specifically, we set $N = 50$ during training. On average, the ratio $\|\nabla_W g(W^t, x^t)\|/\|\nabla_W g(W^t, z_N^t)\|$ exceeds 100, despite some fluctuations. Under these conditions, the term $\nabla_W g(W, z_N^t)$ can be safely neglected, thereby eliminating the need for the expensive loop in Equation (4). This approximation has been effectively utilized in large-scale applications, such as fine-tuning large language models, to reduce memory and computational costs (Shen et al., 2024a). It also serves as a foundation for our proposed algorithm, Loss Discrepancy Control for Multi-Task Learning (LDC-MTL), described in Algorithm 1. LDC-MTL employs a fully single-loop structure, which requires only a single gradient computation for both variables per epoch, resulting in a $\mathcal{O}(1)$ time and memory cost. In Section 6, we show that our LDC-MTL method attains both an ϵ -accurate stationary point for the bilevel problem in eq. (1) and an ϵ -accurate Pareto stationary point for the original loss functions under mild conditions.

5 Empirical Results

In this section, we conduct extensive practical experiments under multi-task classification, regression, and mixed settings to demonstrate the effectiveness of our method. Full experimental details can be found in Appendix A. All experiments are conducted on one NVIDIA A6000 GPU.

Baselines and evaluation. To demonstrate the effectiveness of our proposed method, we evaluate its performance against a broad range of baseline approaches. The compared methods include scalarization-based algorithms, such as Linear Scalarization (LS), Scale-Invariant (SI), Random Loss Weighting (RLW) (Lin et al., 2021), Dynamic Weight Average (DWA) (Liu et al., 2019), Uncertainty Weighting (UW) (Kendall et al., 2018), FAMO (Liu et al., 2024), and GO4Align (Shen et al., 2024b). We also benchmark against gradient manipulation methods, including Multi-Gradient Descent Algorithm (MGDA) (Désidéri, 2012), PCGrad (Yu et al., 2020), GradDrop (Chen et al., 2020), CAGrad (Liu et al., 2021a), IMTL-G (Liu et al., 2021b), MoCo (Fernando et al., 2023), Nash-MTL (Navon et al., 2022), and FairGrad (Ban & Ji, 2024). To provide a comprehensive evaluation, we report the performance of each individual task and employ one additional metric: $\Delta m\%$ to quantify overall performance (Maninis et al., 2019). The $\Delta m\%$ metric measures the average relative performance drop of a multi-task model compared to its corresponding single-task learning (STL). Formally, it is defined as: $\Delta m\% = \frac{1}{K} \sum_{i=1}^K (-1)^{\delta_k} (M_{m,k} - M_{b,k}) / M_{b,k} \times 100$, where $M_{m,k}$ and $M_{b,k}$ represent the performance of the k -th task for the multi-task model m and single-task model b , respectively. The indicator $\delta_k = 1$ if higher values indicate better performance and 0 otherwise.

Table 1: Results on Cityscapes (2-task) dataset. Each experiment is repeated 3 times with different random seeds, and the average is reported. The best results are highlighted in **bold**, while the second-best results are indicated with underlines. Following prior works (Liu et al., 2021a; Fernando et al., 2023; Xiao et al., 2024; Ban & Ji, 2024), we report the mean values of $\Delta m\%$ for all results in the main text, with standard deviations provided in Appendix A.

METHOD	SEGMENTATION		DEPTH		$\Delta m\% \downarrow$
	mIoU \uparrow	PIX ACC \uparrow	ABS ERR \downarrow	REL ERR \downarrow	
STL	74.01	93.16	0.0125	27.77	
LS	75.18	93.49	0.0155	46.77	22.60
SI	70.95	91.73	0.0161	33.83	14.11
RLW (LIN ET AL., 2021)	74.57	93.41	0.0158	47.79	24.38
DWA (LIU ET AL., 2019)	75.24	93.52	0.0160	44.37	21.45
UW (KENDALL ET AL., 2018)	72.02	92.85	0.0140	30.13	5.89
FAMO (LIU ET AL., 2024)	74.54	93.29	0.0145	32.59	8.13
GO4ALIGN (SHEN ET AL., 2024B)	72.63	93.03	0.0164	<u>27.58</u>	8.11
MGDA (DÉSIDÉRI, 2012)	68.84	91.54	0.0309	33.50	44.14
PCGRAD (YU ET AL., 2020)	75.13	93.48	0.0154	42.07	18.29
GRADDROP (CHEN ET AL., 2020)	75.27	93.53	0.0157	47.54	23.73
CAGRAD (LIU ET AL., 2021A)	75.16	93.48	0.0141	37.60	11.64
IMTL-G (LIU ET AL., 2021B)	75.33	93.49	0.0135	38.41	11.10
MoCo (FERNANDO ET AL., 2023)	<u>75.42</u>	93.55	0.0149	34.19	9.90
NASH-MTL (NAVON ET AL., 2022)	75.41	<u>93.66</u>	<u>0.0129</u>	35.02	6.82
FAIRGRAD (BAN & JI, 2024)	75.72	93.68	0.0134	32.25	<u>5.18</u>
LDC-MTL	74.53	93.42	0.0128	26.79	-0.57

5.1 Experimental results

Results on the four benchmark datasets are provided in Table 1, Table 2, Table 7, and Table 8 in the appendix. We observe that LDC-MTL outperforms existing methods on both the CelebA and QM9 datasets, achieving the lowest performance drops of $\Delta m\% = -1.31$ and $\Delta m\% = 49.5$, respectively. Detailed results for the QM9 dataset illustrate that it achieves a balanced performance across all tasks. These results highlight the effectiveness of our method in handling a large number of tasks in both classification and regression settings. Meanwhile, it achieves the lowest performance drop, with $\Delta m\% = -0.57$ on the Cityscapes dataset, while delivering comparable results on the NYU-v2 dataset, where the detailed results are shown in Table 8 in the appendix. These findings highlight the capability of LDC-MTL to effectively handle mixed multi-task learning scenarios.

Efficiency comparison. We compare the running time of well-performing approaches in Figure 3. In particular, our method introduces negligible overhead compared to LS with at most a $1.11\times$ increase, aligning with other $\mathcal{O}(1)$ methods such as GO4Align and FAMO. In contrast, gradient manipulation methods, which take the computational cost $\mathcal{O}(K)$, become significantly slower in many-task scenarios. For example, Nash-MTL requires approximately $12\times$ more training time than LDC-MTL on the CelebA dataset.

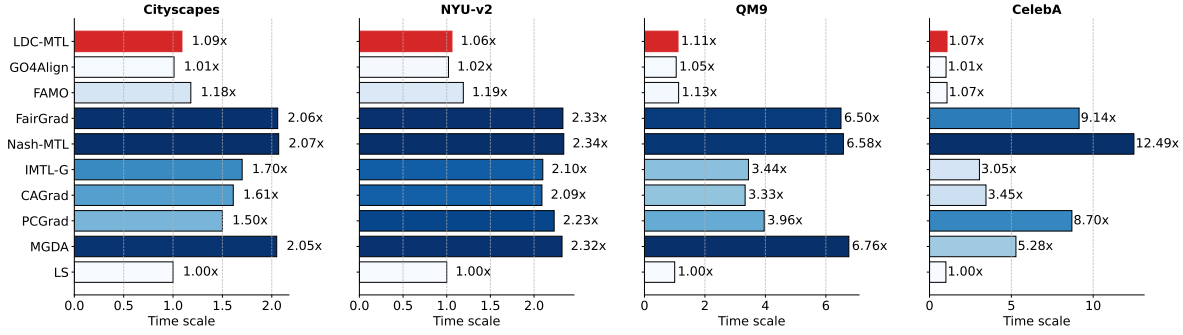


Figure 3: Time scale comparison among well-performing approaches, with LS considered the reference method for standard time.

5.2 Experimental analysis

Loss discrepancy and gradient conflict. To demonstrate the effectiveness of our bilevel formulation for loss discrepancy control, we conduct a detailed analysis of the loss distribution on the CelebA dataset, comparing linear scalarization (LS) with our proposed method. As shown in Figure 4 (left) and statistics in Table 3, the distribution of all 40 task-specific losses reveals that our approach yields more concentrated and consistently lower values. Moreover, we randomly select 8 out of 40 tasks and check the gradient cosine similarity among them. Figure 4 (right) illustrates the cosine similarities of task gradients after the 15th epoch, which shows that the gradient conflict is mitigated as well using our LDC-MTL.

Comparison with weight-swept LS. Prior work has noted that certain multi-task learning methods, such as RLW and PCGrad, do not outperform LS, which can approximate the Pareto front through weight sweeping (Kurin et al., 2022; Xin et al., 2022). To this end, we conduct a careful comparison between our LDC-MTL and LS with weight sweeping on the Cityscapes dataset. From Table 10 in the appendix, even after careful weight sweeping, LS does not outperform our approach. Furthermore, the scatter plot in Figure 5 (a-b) illustrates that LDC-MTL solutions form the Pareto frontier.

Impact of task weight. To further investigate the importance of dynamic weighting, we provide the evolution of task weights for the 11 tasks on the QM9 dataset in Figure 5 (right). It is evident that the task weights adapt meaningfully during the early stages of training and gradually converge later on. Besides, the converged weights are nearly equal, recovering to LS. However, LS does not perform well as shown in Table 7. These findings suggest that, for dynamic-weight methods, the *training trajectory*, not just the final weights, plays a critical role in achieving strong performance.

Table 2: Results on CelebA (40-task), QM9 (11-task), and NYU-v2 (3-task) datasets. Each experiment is repeated 3 times, and the average is reported. The best results are in **bold**, and the second-best results are underlined.

Method	CelebA	QM9	NYU-v2
	$\Delta m\% \downarrow$	$\Delta m\% \downarrow$	$\Delta m\% \downarrow$
LS	4.15	177.6	5.59
SI	7.20	77.8	4.39
RLW (Lin et al., 2021)	1.46	203.8	7.78
DWA (Liu et al., 2019)	3.20	175.3	3.57
UW (Kendall et al., 2018)	3.23	108.0	4.05
FAMO (Liu et al., 2024)	1.21	58.5	-4.10
GO4Align (Shen et al., 2024b)	0.88	<u>52.7</u>	-6.08
MGDA (Désidéri, 2012)	14.85	120.5	1.38
PCGrad (Yu et al., 2020)	3.17	125.7	3.97
CAGrad (Liu et al., 2021a)	2.48	112.8	0.20
IMTL-G (Liu et al., 2021b)	0.84	77.2	-0.76
Nash-MTL (Navon et al., 2022)	2.84	62.0	-4.04
FairGrad (Ban & Ji, 2024)	<u>0.37</u>	57.9	<u>-4.66</u>
LDC-MTL	-1.31	49.5	-4.40

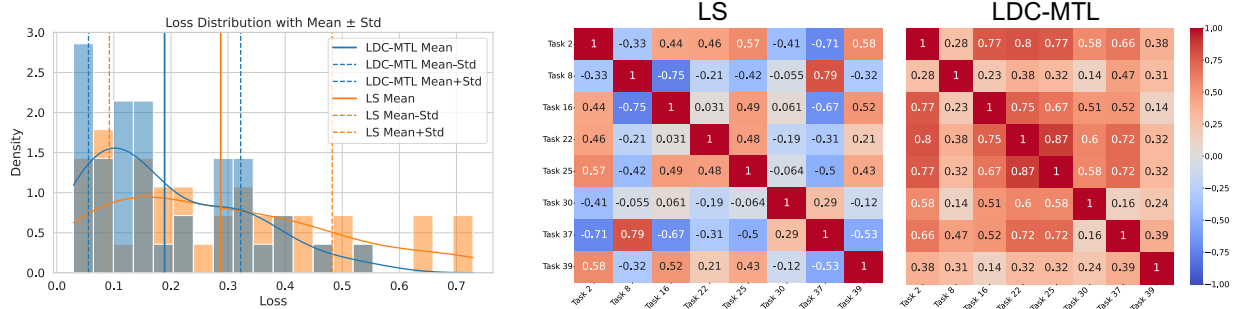


Figure 4: Left: comparison of loss distributions for LDC-MTL and LS on the CelebA dataset. Right: cosine similarities of task gradients for LS and LDC-MTL, respectively; LDC-MTL exhibits much higher gradient similarity among tasks, suggesting reduced gradient conflict.

Hyperparameter sensitivity. In our method, hyperparameters include the step size α and the penalty constant λ . For the step size, we adopt the settings from prior experiments without extensive tuning. While we use the same step size for updates to both W and x in our implementation, these can be adjusted independently in practice. For λ , we determine the optimal value through a grid search and provide additional experimental results on both CelebA and Cityscapes datasets over different λ in Table 4 and Table 9 in the appendix.

Ablation study. We conduct an ablation study to evaluate the impact of normalization and loss discrepancy control (LDC) in our framework. Removing either component leads to performance degradation across tasks, while removing both reduces to LS. The results in Table 5 confirm their complementary benefits.

6 Theoretical Analysis

In this section, we provide convergence analysis for our LDC-MTL method. We first provide several useful definitions and assumptions.

Definition 1. Given $L > 0$, a function ℓ is said to be L -Lipschitz-continuous on \mathcal{X} if it holds for any $x, x' \in \mathcal{X}$ that $\|\ell(x) - \ell(x')\| \leq L\|x - x'\|$. A function ℓ is said to be L -Lipschitz-smooth if its gradient is L -Lipschitz-continuous.

Definition 2 (Pareto stationarity). We say x is an ϵ -accurate Pareto stationary point for loss functions $\{l_i(x)\}$ if $\min_{w \in \mathcal{W}} \|G(x)w\|^2 = \mathcal{O}(\epsilon)$, where $G(x) = [\nabla l_1(x), \nabla l_2(x), \dots, \nabla l_K(x)]^\top$.

Table 3: Statistics of loss values for LDC-MTL and LS on the CelebA dataset. Lower mean and std indicate better and more stable performance.

Method	Mean ↓	Std ↓	Min	Max
LDC-MTL	0.1888	0.1333	0.0292	0.5384
LS	0.2872	0.1952	0.0320	0.7289

Table 4: Parameter tuning results on the CelebA dataset.

Method	$\Delta m\% \downarrow$
FairGrad (Ban & Ji, 2024)	0.37
LDC-MTL ($\lambda = 0.005$)	-1.27
LDC-MTL ($\lambda = 0.008$)	-1.16
LDC-MTL ($\lambda = 0.01$)	-1.31
LDC-MTL ($\lambda = 0.02$)	-0.96

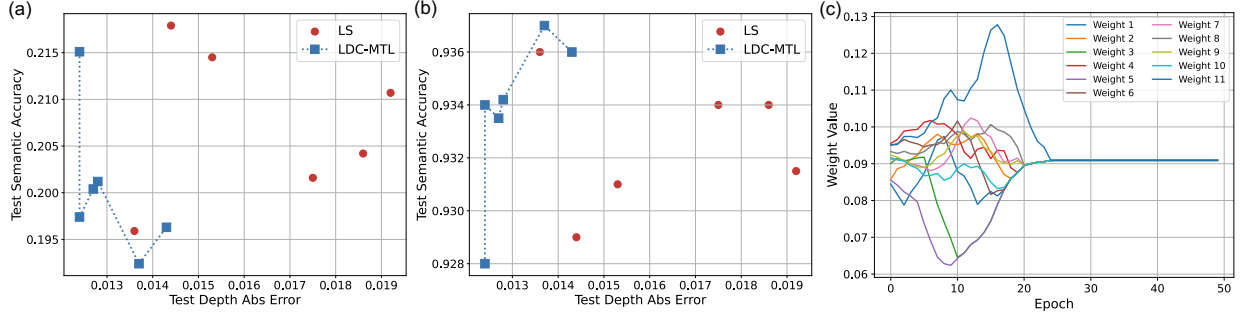


Figure 5: Comparison between LS and LDC-MTL on the Cityscapes dataset (a–b). (a) Test segmentation loss vs. test depth loss: points closer to the lower left indicate better performance. (b) Test pixel accuracy vs. absolute depth estimation error: points in the upper left indicate better performance. In both cases, LDC-MTL solutions lie on the Pareto frontier. (c) Weight change of 11 tasks using LDC-MTL during the training on the QM9 dataset.

Inspired by Shen & Chen 2023, we define the following two surrogates of the original bilevel problem in eq. (1).

Definition 3. Define two surrogate bilevel problems as

$$\begin{aligned} \mathcal{BP}_\lambda &: \min_{W,x} f(W,x) + \lambda(g(W,x) - g(W,x^*)), \\ \mathcal{BP}_\epsilon &: \min_{W,x} f(W,x) \text{ s.t. } g(W,x) - g(W,x^*) \leq \epsilon, \end{aligned}$$

where \mathcal{BP}_λ is the penalized bilevel problem, and \mathcal{BP}_ϵ recovers to the original problem if $\epsilon = 0$.

Assumption 1 (Lipschitz and smoothness). *There exists a constant L such that the upper-level function $f(W, \cdot)$ is L -Lipschitz continuous. There exists constants L_f and L_g such that functions $f(W, x)$ and $g(W, x)$ are L_f - and L_g -Lipschitz-smooth.*

Assumption 2 (Polyak-Lojasiewicz (PL) condition). *The lower-level function $g(W, \cdot)$ satisfies the $\frac{1}{\mu}$ -PL condition if there exists a $\mu > 0$ such that given any W , it holds for any feasible x that $\|\nabla_x g(W, x)\|^2 \geq \frac{1}{\mu}(g(W, x) - g(W, x^*))$.*

Lipschitz continuity and smoothness are standard assumptions in the study of bilevel optimization (Ghadimi & Wang, 2018; Ji et al., 2021). While the absolute values in the upper-level function in Equation (1) are non-smooth, they can be easily modified to ensure smoothness, such as by using a soft absolute value function of the form $y = \sqrt{x^2 + \gamma}$ where γ is a small positive constant. Moreover, the PL condition can be satisfied in over-parameterized neural network settings (Mei et al., 2020; Frei & Gu, 2021). The following theorem presents the convergence analysis of our algorithms.

Theorem 1. Suppose Assumptions 1- 2 are satisfied. Select hyperparameters

$$\alpha \in \left(0, \frac{1}{L_f + \lambda(2L_g + L_g^2\mu)}\right], \beta \in \left(0, \frac{1}{L_g}\right], \lambda = L\sqrt{3\mu\epsilon^{-1}}, \text{ and } N = \Omega(\log(\alpha t)).$$

Table 5: Ablation study on normalization (Norm.) and loss discrepancy control (LDC). $\Delta m\%$ is used as the metric.

Norm.	LDC	NYU-v2	QM9
✓	✓	-4.40	49.5
✗	✓	-2.43	125.4
✓	✗	-3.00	89.57
✗	✗	5.59	177.6

(i) Our method with the updates eq. (3) and eq. (4) (i.e., Algorithm 2 in the appendix) finds an ϵ -accurate stationary point of the problem \mathcal{BP}_λ . If this stationary point is a local/global solution to \mathcal{BP}_λ , it is also a local/global solution to \mathcal{BP}_ϵ . Furthermore, it is also an ϵ -accurate Pareto stationary point for loss functions $l_i(x), i = 1, \dots, K$.

(ii) Moreover, if $\|\nabla_W g(W^t, z_N^t)\| = \mathcal{O}(\epsilon)$ for $t = 1, \dots, T$. The simplified method in Algorithm 1 also achieves the same convergence guarantee as that in (i).

The complete proof is provided in Theorem 2. In the first part of our theorem, we establish a connection between the stationarity of \mathcal{BP}_λ and Pareto stationarity, as well as an equivalence between the Pareto stationarities of the original loss functions $\{l_i\}$ and the normalized loss functions $\{\tilde{l}_i\}$. The second part of Theorem 1 introduces an additional gradient vanishing assumption, which has been validated in our experiments. It demonstrates that our simplified LDC-MTL method can also attain an ϵ -accurate stationary point for the problem \mathcal{BP}_λ and an ϵ -accurate Pareto stationary point for the original loss functions.

7 Conclusion

We introduced LDC-MTL, a scalable loss discrepancy control approach for multi-task learning based on bilevel optimization. Our method achieves efficient loss discrepancy control with only $\mathcal{O}(1)$ time and memory complexity while guaranteeing convergence to both a stationary point of the bilevel problem and an ϵ -accurate Pareto stationary point for all task loss functions. Extensive experiments demonstrate that LDC-MTL outperforms existing methods in both accuracy and efficiency, highlighting its effectiveness for large-scale MTL. For future work, we plan to explore the application of our method to broader multi-task learning problems, including recommendation systems.

References

- Idan Achituve, Idit Diamant, Arnon Netzer, Gal Chechik, and Ethan Fetaya. Bayesian uncertainty for gradient aggregation in multi-task learning. *arXiv preprint arXiv:2402.04005*, 2024.
- Vijay Badrinarayanan, Alex Kendall, and Roberto Cipolla. Segnet: A deep convolutional encoder-decoder architecture for image segmentation. *IEEE Transactions on Pattern Analysis and Machine Intelligence*, 39(12):2481–2495, 2017.
- Hao Ban and Kaiyi Ji. Fair resource allocation in multi-task learning. *arXiv preprint arXiv:2402.15638*, 2024.
- Jerome Bracken and James T McGill. Mathematical programs with optimization problems in the constraints. *Operations Research*, 21(1):37–44, 1973.
- Rich Caruana. Multitask learning. *Machine Learning*, 28:41–75, 1997.
- Lesi Chen, Jing Xu, and Jingzhao Zhang. Bilevel optimization without lower-level strong convexity from the hyper-objective perspective. *arXiv preprint arXiv:2301.00712*, 2023.
- Lisha Chen, Heshan Fernando, Yiming Ying, and Tianyi Chen. Three-way trade-off in multi-objective learning: Optimization, generalization and conflict-avoidance. *Advances in Neural Information Processing Systems*, 36, 2024.

- Yaran Chen, Dongbin Zhao, Le Lv, and Qichao Zhang. Multi-task learning for dangerous object detection in autonomous driving. *Information Sciences*, 432:559–571, 2018.
- Zhao Chen, Jiquan Ngiam, Yanping Huang, Thang Luong, Henrik Kretzschmar, Yuning Chai, and Dragomir Anguelov. Just pick a sign: Optimizing deep multitask models with gradient sign dropout. *Advances in Neural Information Processing Systems*, 33:2039–2050, 2020.
- Marius Cordts, Mohamed Omran, Sebastian Ramos, Timo Rehfeld, Markus Enzweiler, Rodrigo Benenson, Uwe Franke, Stefan Roth, and Bernt Schiele. The cityscapes dataset for semantic urban scene understanding. In *Proceedings of the IEEE Conference on Computer Vision and Pattern Recognition*, pp. 3213–3223, 2016.
- Yanqi Dai, Nanyi Fei, and Zhiwu Lu. Improvable gap balancing for multi-task learning. In *Uncertainty in Artificial Intelligence*, pp. 496–506. PMLR, 2023.
- Jean-Antoine Désidéri. Multiple-gradient descent algorithm (mgda) for multiobjective optimization. *Comptes Rendus Mathématique*, 350(5-6):313–318, 2012.
- Justin Domke. Generic methods for optimization-based modeling. In *Artificial Intelligence and Statistics*, pp. 318–326. PMLR, 2012.
- Heshan Fernando, Han Shen, Miao Liu, Subhajit Chaudhury, Keerthiram Murugesan, and Tianyi Chen. Mitigating gradient bias in multi-objective learning: A provably convergent approach. In *International Conference on Learning Representations*, 2023.
- Luca Franceschi, Michele Donini, Paolo Frasconi, and Massimiliano Pontil. Forward and reverse gradient-based hyperparameter optimization. In *International Conference on Machine Learning*, pp. 1165–1173. PMLR, 2017.
- Spencer Frei and Quanquan Gu. Proxy convexity: A unified framework for the analysis of neural networks trained by gradient descent. *Advances in Neural Information Processing Systems*, 34:7937–7949, 2021.
- Saeed Ghadimi and Mengdi Wang. Approximation methods for bilevel programming. *arXiv preprint arXiv:1802.02246*, 2018.
- Pierre Hansen, Brigitte Jaumard, and Gilles Savard. New branch-and-bound rules for linear bilevel programming. *SIAM Journal on Scientific and Statistical Computing*, 13(5):1194–1217, 1992.
- Kaiyi Ji, Junjie Yang, and Yingbin Liang. Bilevel optimization: Convergence analysis and enhanced design. In *International Conference on Machine Learning*, pp. 4882–4892. PMLR, 2021.
- Alex Kendall, Yarin Gal, and Roberto Cipolla. Multi-task learning using uncertainty to weigh losses for scene geometry and semantics. In *Proceedings of the IEEE Conference on Computer Vision and Pattern Recognition*, pp. 7482–7491, 2018.
- Iasonas Kokkinos. Ubertnet: Training a universal convolutional neural network for low-, mid-, and high-level vision using diverse datasets and limited memory. In *Proceedings of the IEEE Conference on Computer Vision and Pattern Recognition*, pp. 6129–6138, 2017.

- Vitaly Kurin, Alessandro De Palma, Ilya Kostrikov, Shimon Whiteson, and Pawan K Mudigonda. In defense of the unitary scalarization for deep multi-task learning. *Advances in Neural Information Processing Systems*, 35:12169–12183, 2022.
- Jeongyeol Kwon, Dohyun Kwon, Stephen Wright, and Robert D Nowak. A fully first-order method for stochastic bilevel optimization. In *International Conference on Machine Learning*, pp. 18083–18113. PMLR, 2023.
- Baijiong Lin, Feiyang Ye, Yu Zhang, and Ivor W Tsang. Reasonable effectiveness of random weighting: A litmus test for multi-task learning. *arXiv preprint arXiv:2111.10603*, 2021.
- Bo Liu, Xingchao Liu, Xiaojie Jin, Peter Stone, and Qiang Liu. Conflict-averse gradient descent for multi-task learning. *Advances in Neural Information Processing Systems*, 34:18878–18890, 2021a.
- Bo Liu, Yihao Feng, Peter Stone, and Qiang Liu. Famo: Fast adaptive multitask optimization. *Advances in Neural Information Processing Systems*, 36, 2024.
- Liyang Liu, Yi Li, Zhanghui Kuang, J Xue, Yimin Chen, Wenming Yang, Qingmin Liao, and Wayne Zhang. Towards impartial multi-task learning. In *Proceedings of the International Conference on Learning Representations (ICLR) 2021*, 2021b.
- Shikun Liu, Edward Johns, and Andrew J Davison. End-to-end multi-task learning with attention. In *Proceedings of the IEEE/CVF Conference on Computer Vision and Pattern Recognition*, pp. 1871–1880, 2019.
- Ziwei Liu, Ping Luo, Xiaogang Wang, and Xiaoou Tang. Deep learning face attributes in the wild. In *Proceedings of the IEEE International Conference on Computer Vision*, pp. 3730–3738, 2015.
- Dougal Maclaurin, David Duvenaud, and Ryan Adams. Gradient-based hyperparameter optimization through reversible learning. In *International Conference on Machine Learning*, pp. 2113–2122. PMLR, 2015.
- Kevis-Kokitsi Maninis, Ilija Radosavovic, and Iasonas Kokkinos. Attentive single-tasking of multiple tasks. In *Proceedings of the IEEE/CVF conference on computer vision and pattern recognition*, pp. 1851–1860, 2019.
- Jincheng Mei, Chenjun Xiao, Csaba Szepesvari, and Dale Schuurmans. On the global convergence rates of softmax policy gradient methods. In *International Conference on Machine Learning*, pp. 6820–6829. PMLR, 2020.
- Aviv Navon, Aviv Shamsian, Idan Achituve, Haggai Maron, Kenji Kawaguchi, Gal Chechik, and Ethan Fetaya. Multi-task learning as a bargaining game. *arXiv preprint arXiv:2202.01017*, 2022.
- Raghunathan Ramakrishnan, Pavlo O Dral, Matthias Rupp, and O Anatole Von Lilienfeld. Quantum chemistry structures and properties of 134 kilo molecules. *Scientific Data*, 1(1):1–7, 2014.
- Sebastian Ruder, Joachim Bingel, Isabelle Augenstein, and Anders Søgaard. Latent multi-task architecture learning. In *Proceedings of the AAAI Conference on Artificial Intelligence*, volume 33, pp. 4822–4829, 2019.
- Ozan Sener and Vladlen Koltun. Multi-task learning as multi-objective optimization. *Advances in Neural Information Processing Systems*, 31, 2018.

- Han Shen and Tianyi Chen. On penalty-based bilevel gradient descent method. In *International Conference on Machine Learning*, pp. 30992–31015. PMLR, 2023.
- Han Shen, Pin-Yu Chen, Payel Das, and Tianyi Chen. Seal: Safety-enhanced aligned llm fine-tuning via bilevel data selection. *arXiv preprint arXiv:2410.07471*, 2024a.
- Jiayi Shen, Cheems Wang, Zehao Xiao, Nanne Van Noord, and Marcel Worring. Go4align: Group optimization for multi-task alignment. *arXiv preprint arXiv:2404.06486*, 2024b.
- Chenggen Shi, Jie Lu, and Guangquan Zhang. An extended kuhn–tucker approach for linear bilevel programming. *Applied Mathematics and Computation*, 162(1):51–63, 2005.
- Nathan Silberman, Derek Hoiem, Pushmeet Kohli, and Rob Fergus. Indoor segmentation and support inference from rgb-d images. In *Computer Vision—ECCV 2012: 12th European Conference on Computer Vision, Florence, Italy, October 7–13, 2012, Proceedings, Part V 12*, pp. 746–760. Springer, 2012.
- Menghan Wang, Yujie Lin, Guli Lin, Keping Yang, and Xiao-ming Wu. M2grl: A multi-task multi-view graph representation learning framework for web-scale recommender systems. In *Proceedings of the 26th ACM SIGKDD International Conference on Knowledge Discovery & Data Mining*, pp. 2349–2358, 2020.
- Yudan Wang, Peiyao Xiao, Hao Ban, Kaiyi Ji, and Shaofeng Zou. Finite-time analysis for conflict-avoidant multi-task reinforcement learning. *arXiv preprint arXiv:2405.16077*, 2024.
- Peiyao Xiao and Kaiyi Ji. Communication-efficient federated hypergradient computation via aggregated iterative differentiation. In *International Conference on Machine Learning*, pp. 38059–38086. PMLR, 2023.
- Peiyao Xiao, Hao Ban, and Kaiyi Ji. Direction-oriented multi-objective learning: Simple and provable stochastic algorithms. *Advances in Neural Information Processing Systems*, 36, 2024.
- Derrick Xin, Behrooz Ghorbani, Justin Gilmer, Ankush Garg, and Orhan Firat. Do current multi-task optimization methods in deep learning even help? *Advances in neural information processing systems*, 35: 13597–13609, 2022.
- Yifan Yang, Peiyao Xiao, and Kaiyi Ji. Achieving $\mathcal{O}(\epsilon^{-1.5})$ complexity in hessian/jacobian-free stochastic bilevel optimization. *arXiv preprint arXiv:2312.03807*, 2023.
- Yifan Yang, Hao Ban, Minhui Huang, Shiqian Ma, and Kaiyi Ji. Tuning-free bilevel optimization: New algorithms and convergence analysis. *arXiv preprint arXiv:2410.05140*, 2024a.
- Yifan Yang, Peiyao Xiao, and Kaiyi Ji. Simfbo: Towards simple, flexible and communication-efficient federated bilevel learning. *Advances in Neural Information Processing Systems*, 36, 2024b.
- Tianhe Yu, Saurabh Kumar, Abhishek Gupta, Sergey Levine, Karol Hausman, and Chelsea Finn. Gradient surgery for multi-task learning. *Advances in Neural Information Processing Systems*, 33:5824–5836, 2020.
- Zhihan Zhang, Wenhao Yu, Mengxia Yu, Zhichun Guo, and Meng Jiang. A survey of multi-task learning in natural language processing: Regarding task relatedness and training methods. *arXiv preprint arXiv:2204.03508*, 2022.
- Shiji Zhou, Wenpeng Zhang, Jiyan Jiang, Wenliang Zhong, Jinjie Gu, and Wenwu Zhu. On the convergence of stochastic multi-objective gradient manipulation and beyond. *Advances in Neural Information Processing Systems*, 35:38103–38115, 2022.

A Experiment details

A.1 Experimental setup

Image-Level Classification. CelebA (Liu et al., 2015), one of the most widely used datasets, is a large-scale facial attribute dataset containing over 200K celebrity images. Each image is annotated with 40 attributes, such as the presence of eyeglasses and smiling. Following the experimental setup in Ban & Ji 2024, we treat CelebA as a 40-task multi-task learning (MTL) classification problem, where each task predicts the presence of a specific attribute. Since all tasks involve binary classification with the same *binary cross-entropy* loss function, we do not apply any normalization for both options of $\tau = 1$ and $\tau = \sigma$ at the coarse loss pre-normalization stage. The network architecture consists of a 9-layer convolutional neural network (CNN) as the shared model, with multiple linear layers serving as task-specific heads. We train the model for 15 epochs using the Adam optimizer with a batch size of 256.

Regression. QM9 (Ramakrishnan et al., 2014) dataset is another widely used benchmark for multi-task regression problems in quantum chemistry. It contains 130K molecules represented as graphs, and 11 properties to be predicted. Though all tasks share the same loss function, *mean squared error*, they exhibit varying scales: a phenomenon commonly observed in regression tasks but less prevalent in classification tasks, as shown in Figure 6. To address this scale discrepancy, we adopt the logarithmic normalization in Section 4.1 at the coarse loss pre-normalization stage for both options of $\tau = 1$ and $\tau = \sigma$. Following the experimental setup in Liu et al. 2024; Navon et al. 2022, we use the same model and data split, 110K molecules for training, 10k for validation, and the rest 10k for testing. The model is trained for 300 epochs with a batch size of 120. The learning rate starts at 1e-3 and is reduced whenever the validation performance stagnates for 5 consecutive epochs.

Dense Prediction. The Cityscapes dataset (Cordts et al., 2016) consists of 5000 street-scene images designed for two tasks: 7-class semantic segmentation (a classification task) and depth estimation (a regression task). Similarly, the NYU-v2 dataset (Silberman et al., 2012) is widely used for indoor scene understanding and contains 1449 densely annotated images. It includes one pixel-level classification task, semantic segmentation, and two pixel-level regression tasks, 13-class depth estimation, plus surface normal prediction. These datasets provide benchmarks for evaluating the performance of our method in mixed multi-task settings. Since the number of tasks is small and the loss values exhibit minimal variation, we applied rescaled normalization when selecting $\tau = \sigma$ and no normalization when selecting $\tau = 1$. We follow the same experimental setup described in Liu et al. 2021a; Navon et al. 2022 and adopt MTAN (Liu et al., 2019) as the backbone, which incorporates task-specific attention modules into SegNet (Badrinarayanan et al., 2017). Both models are trained for 200 epochs, with batch sizes of 8 for Cityscapes and 8 for NYU-v2. The learning rates are initialized at 3e-4 and 1e-4 for the first 100 epochs and reduced by half for the remaining epochs, respectively.

In a word, the hyperparameter choices are summarized in Table 6.

Table 6: Training hyperparameters combination and the best results per dataset.

Dataset	Stepsize	Penalty constant	τ	$\Delta m\%$
CelebA	1e-03	0.01	$\sigma(W)$	-1.31 \pm 0.26
QM9	1e-03	0.05	$\sigma(W)$	49.5 \pm 3.64
Cityscapes	3e-04	0.1	1	-0.57 \pm 1.17
NYU-v2	8e-05	0.05	1	-4.40 \pm 0.74

A.2 Loss and gradient scales

To validate the necessity of normalization, we show that loss can vary significantly in scale. For example, as shown in Figure 6, we observed that the loss values during training across 11 regression tasks in the QM9 dataset exhibit substantial differences in magnitude, with loss ratios exceeding 1000 in certain instances. Moreover, we have also drawn the loss progression over time of LS. Tasks 1–4 are easier to optimize and dominate the training when using linear scalarization, leading other tasks to converge suboptimally. In contrast, LDC-MTL accounts for loss scale and adaptively reweights tasks using bilevel optimization, enabling better balance. For example, tasks 6–10 improve their final loss scale from 10^{-3} to 10^{-5} . This result provides empirical insights supporting the importance of normalization in multi-task learning (MTL) problems.

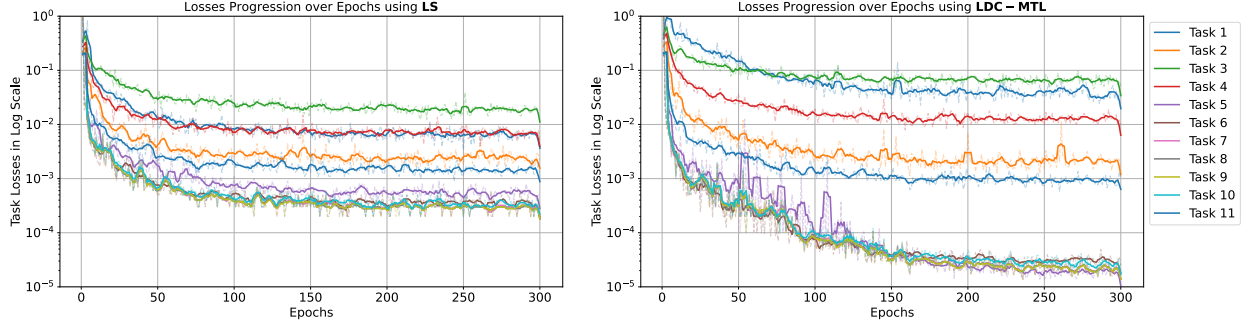


Figure 6: Curves of loss values during the training process for all 11 tasks on the QM9 dataset using different methods. The loss values vary significantly across different tasks. For LS, some tasks converge suboptimally due to the loss discrepancy.

Moreover, our experiments reveal that the gradient norm $\|\nabla_W g(W^t, z_N^t)\|$ remains sufficiently small, typically orders of magnitude smaller than the gradient norm $\|\nabla_W g(W^t, x^t)\|$, which is used to update outer parameters W . This behavior is illustrated in Figure 7. Specifically, we set $N = 50$ during training. In average, the ratio $\|\nabla_W g(W^t, x^t)\|/\|\nabla_W g(W^t, z_N^t)\|$ exceeds 100, despite some fluctuations.

A.3 Toy example

To better understand the benefits of our method, we illustrate the training trajectory along with the training time in a toy example of 2-task learning following the same setting in FAMO (Liu et al., 2024). The loss functions $L_1(x), L_2(x)$, where x is the model parameter, of two tasks are listed below.

$$\begin{aligned}
 L_1(x) &= 0.1 \times (c_1(x)f_1(x) + c_2(x)g_1(x)), \quad L_2(x) = c_1(x)f_2(x) + c_2(x)g_2(x) \quad \text{where} \\
 f_1(x) &= \log(\max(|0.5(-x_1 - 7) - \tanh(-x_2)|, 0.000005)) + 6, \\
 f_2(x) &= \log(\max(|0.5(-x_1 + 3) - \tanh(-x_2) + 2|, 0.000005)) + 6, \\
 g_1(x) &= ((-x_1 + 7)^2 + 0.1 * (-x_2 - 8)^2)/10 - 20, \\
 g_2(x) &= ((-x_1 - 7)^2 + 0.1 * (-x_2 - 8)^2)/10 - 20, \\
 c_1(x) &= \max(\tanh(0.5 * x_2), 0) \quad \text{and} \quad c_2(x) = \max(\tanh(-0.5 * x_2), 0).
 \end{aligned} \tag{5}$$

In Figure 1, the black dots represent 5 chosen initial points $\{(-8.5, 7.5), (-8.5, 5), (0, 0), (9, 9), (10, -8)\}$ while the black stars represent the converging points on the Pareto front. We use the Adam optimizer and train each method for 50k steps. Our method can always converge to balanced results efficiently. We use

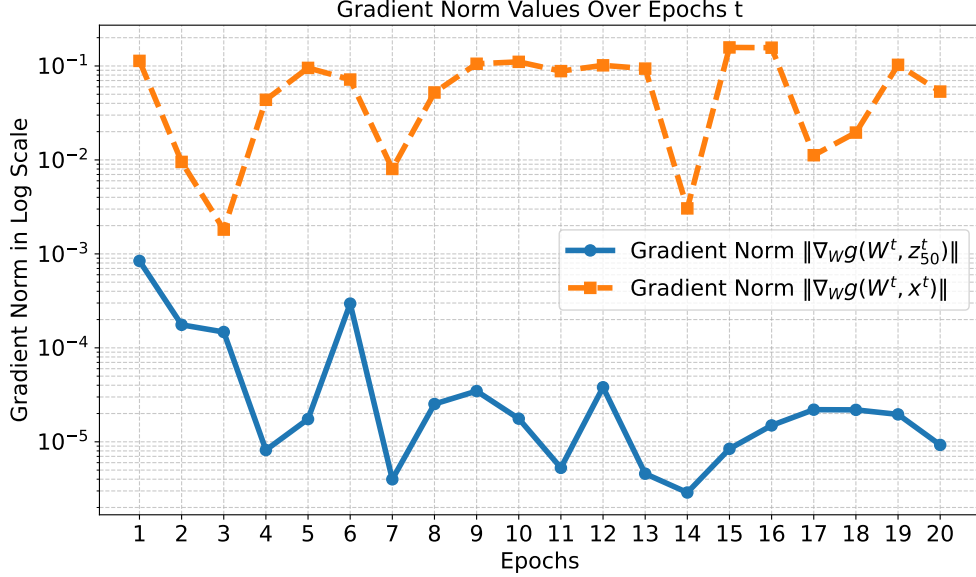


Figure 7: Gradient norm values during the training process on the Cityscapes dataset. Similar phenomena have also been observed in other datasets.

Adam optimizer with a learning rate of $1e-3$. The training time is recalculated according to real-time ratios in our machine. We find that LS and MGDA do not converge to balanced points, while FAMO converges to balanced results to some extent. Meanwhile, our method with rescale normalization can always converge to balanced results efficiently.

A.4 Detailed results

Here we provide detailed results of NYU-v2 in Table 8 and QM9 in Table 7.

A.5 Parameter tuning

In our experiments, the penalty constant λ requires some tuning effort, whereas the choice of step size had relatively less impact and did not require extensive tuning. We have included additional results on the CelebA and Cityscapes datasets in Table 4 and Table 9 that explore the effect of varying λ , and found that values in the range $\lambda \in [0.02, 0.1]$ consistently yield strong performance.

A.6 Loss discrepancy and gradient conflict

To demonstrate the effectiveness of our bilevel formulation for loss discrepancy control, we conduct a detailed analysis of the loss distribution on the CelebA dataset, comparing linear scalarization (LS) with our proposed method. As shown in Figure 4 (left) and statistics in Table 3, the distribution of all 40 task-specific losses reveals that our approach yields more concentrated and consistently lower values.

Except for the loss discrepancy, we randomly select 8 out of 40 tasks and have checked the gradient cosine similarity among tasks on the CelebA dataset. Figure 4 (right) illustrates the cosine similarities of task gradients after the 15th epoch, which shows that the gradient conflict is mitigated.

Table 7: Detailed results of on QM9 (11-task) dataset. Each experiment is repeated 3 times, and the average is reported. The best results are highlighted in **bold**, while the second-best results are indicated with underlines.

METHOD	μ	α	ϵ_{HOMO}	ϵ_{LUMO}	$\langle R^2 \rangle$	ZPVE	U_0	U	H	G	c_v	$\Delta m\%$ ↓
	MAE ↓											
STL	0.067	0.181	60.57	53.91	0.502	4.53	58.8	64.2	63.8	66.2	0.072	
LS	0.106	0.325	73.57	89.67	5.19	14.06	143.4	144.2	144.6	140.3	0.128	177.6
SI	0.309	0.345	149.8	135.7	<u>1.00</u>	<u>4.50</u>	55.3	55.75	55.82	55.27	0.112	77.8
RLW (LIN ET AL., 2021)	0.113	0.340	76.95	92.76	5.86	15.46	156.3	157.1	157.6	153.0	0.137	203.8
DWA (LIU ET AL., 2019)	0.107	0.325	<u>74.06</u>	90.61	5.09	13.99	142.3	143.0	143.4	139.3	0.125	175.3
UW (KENDALL ET AL., 2018)	0.386	0.425	166.2	155.8	1.06	4.99	66.4	66.78	66.80	66.24	0.122	108.0
FAMO (LIU ET AL., 2024)	0.15	0.30	94.0	95.2	1.63	4.95	70.82	71.2	71.2	70.3	0.10	58.5
GO4ALIGN (SHEN ET AL., 2024B)	0.17	0.35	102.4	119.0	1.22	4.94	<u>53.9</u>	<u>54.3</u>	<u>54.3</u>	<u>53.9</u>	0.11	<u>52.7</u>
MGDA (DÉSIDÉRI, 2012)	0.217	0.368	126.8	104.6	3.22	5.69	88.37	89.4	89.32	88.01	0.120	120.5
PCGRAD (YU ET AL., 2020)	<u>0.106</u>	0.293	75.85	88.33	3.94	9.15	116.36	116.8	117.2	114.5	0.110	125.7
CAGRAD (LIU ET AL., 2021A)	0.118	0.321	83.51	94.81	3.21	6.93	113.99	114.3	114.5	112.3	0.116	112.8
IMTL-G (LIU ET AL., 2021B)	0.136	0.287	98.31	93.96	1.75	5.69	101.4	102.4	102.0	100.1	0.096	77.2
NASH-MTL (NAVON ET AL., 2022)	0.102	0.248	82.95	81.89	2.42	5.38	74.5	75.02	75.10	74.16	0.093	62.0
FAIRGRAD (BAN & JI, 2024)	0.117	<u>0.253</u>	87.57	<u>84.00</u>	2.15	5.07	70.89	71.17	71.21	70.88	<u>0.095</u>	57.9
LDC-MTL	0.23	0.29	123.89	111.95	0.97	3.99	42.73	43.1	43.2	43.1	0.097	49.5±3.64

A.7 Comparison with weight-swept LS

We have operated a weight sweep on linear scalarization, and the result is shown in Table 10. From this table, we find that even after a careful weight sweep, LS does not perform better than our method. Moreover, we have also provided a scatter plot in Figure 5 (left) using results in Table 9 and Table 10 following Figure 8 in Xin et al. 2022. In both cases, our method forms the Pareto frontier.

A.8 Ablation study on task orders

To investigate the impact of loss ordering in the upper-level function $f(W, x^*)$ in Equation (1), we randomly shuffled the order of loss values before computing the (weighted) loss gaps on the CelebA dataset. The results are reported in Table 11 where CelebA_(reorder) represents random reordering on task losses before computing $f(W, x)$. Our findings indicate that reordering the losses does not lead to significant performance differences. This suggests that the effect of task ordering is minimal, likely because the loss values are already on a comparable scale.

B Additional information

Here, we present the complete version of the double-loop algorithm for solving the penalized bilevel problem, \mathcal{BP}_λ in Equation (2), as detailed in Algorithm 2. Notably, the local or global solution of \mathcal{BP}_λ obtained by Algorithm 2 also serves as a local or global solution to \mathcal{BP}_ϵ , as established by Proposition 2 in Shen & Chen 2023.

Table 8: Results on NYU-v2 (3-task) dataset. Each experiment is repeated 3 times with different random seeds, and the average is reported.

METHOD	SEGMENTATION		DEPTH		SURFACE NORMAL					$\Delta m\%$ ↓
	mIoU ↑	Pix Acc ↑	Abs Err ↓	Rel Err ↓	ANGLE DISTANCE ↓		WITHIN t° ↑			
					MEAN	MEDIAN	11.25	22.5	30	
STL	38.30	63.76	0.6754	0.2780	25.01	19.21	30.14	57.20	69.15	
LS	39.29	65.33	0.5493	0.2263	28.15	23.96	22.09	47.50	61.08	5.59
SI	38.45	64.27	<u>0.5354</u>	0.2201	27.60	23.37	22.53	48.57	62.32	4.39
RLW (LIN ET AL., 2021)	37.17	63.77	0.5759	0.2410	28.27	24.18	22.26	47.05	60.62	7.78
DWA (LIU ET AL., 2019)	39.11	65.31	0.5510	0.2285	27.61	23.18	24.17	50.18	62.39	3.57
UW (KENDALL ET AL., 2018)	36.87	63.17	0.5446	0.2260	27.04	22.61	23.54	49.05	63.65	4.05
FAMO (LIU ET AL., 2024)	38.88	64.90	0.5474	0.2194	25.06	19.57	29.21	56.61	68.98	-4.10
GO4ALIGN (SHEN ET AL., 2024B)	40.42	65.37	0.5492	<u>0.2167</u>	<u>24.76</u>	18.94	30.54	57.87	69.84	-6.08
MGDA (DÉSIDÉRI, 2012)	30.47	59.90	0.6070	0.2555	24.88	19.45	29.18	56.88	69.36	1.38
PCGRAD (YU ET AL., 2020)	38.06	64.64	0.5550	0.2325	27.41	22.80	23.86	49.83	63.14	3.97
GRADDROP (CHEN ET AL., 2020)	39.39	65.12	0.5455	0.2279	27.48	22.96	23.38	49.44	62.87	3.58
CAGRAD (LIU ET AL., 2021A)	39.79	65.49	0.5486	0.2250	26.31	21.58	25.61	52.36	65.58	0.20
IMTL-G (LIU ET AL., 2021B)	39.35	65.60	0.5426	0.2256	26.02	21.19	26.20	53.13	66.24	-0.76
MoCo (FERNANDO ET AL., 2023)	<u>40.30</u>	66.07	0.5575	0.2135	26.67	21.83	25.61	51.78	64.85	0.16
NASH-MTL (NAVON ET AL., 2022)	40.13	65.93	0.5261	0.2171	25.26	20.08	28.40	55.47	68.15	-4.04
FAIRGRAD (BAN & JI, 2024)	39.74	<u>66.01</u>	0.5377	0.2236	24.84	19.60	29.26	56.58	69.16	<u>-4.66</u>
LDC-MTL	38.04	38.04	0.5402	0.2278	24.70	<u>19.19</u>	<u>29.97</u>	<u>57.44</u>	<u>69.69</u>	-4.40±0.74

Algorithm 2: Double-loop First-order Method

```

Initialize:  $W^0, x^0, z_0^0$ 
for  $t = 0, 1, \dots, T-1$  do
  Warm start:  $z_0^t = x^t$ 
  for  $n = 0, 1, \dots, N$  do
     $z_{n+1}^t = z_n^t - \beta \lambda \nabla_z g(W^t, z_n^t)$ 
  end for
   $x^{t+1} = x^t - \alpha (\nabla_x f(W^t, x^t) + \lambda \nabla_x g(W^t, x^t))$ 
   $W^{t+1} = W^t - \alpha (\nabla_W f(W^t, x^t) + \lambda (\nabla_W g(W^t, x^t) - \nabla_W g(W^t, z_N^t)))$ 
end for

```

C Analysis

In the analysis, we need the following definitions.

$$\begin{aligned}
x_t^* &= \arg \min_x g(W^t, x), \\
G(x) &= [\nabla l_1(x), \nabla l_2(x), \dots, \nabla l_K(x)], \tilde{G}(x) = [\nabla \tilde{l}_1(x), \nabla \tilde{l}_2(x), \dots, \nabla \tilde{l}_K(x)] \\
F(\theta^t) &= f(\theta^t) + \lambda p(\theta^t), \Phi(\theta^t) = f(\theta^t) + \lambda g(\theta^t), \\
\text{where } \theta^t &= (W^t, x^t), p(\theta^t) = g(W^t, x^t) - g(W^t, x_t^*) \\
\nabla f(W, x) &= (\nabla_W f(W, x), \nabla_x f(W, x)), \nabla g(W, x) = (\nabla_W g(W, x), \nabla_x g(W, x)).
\end{aligned} \tag{6}$$

Lemma 1. *Let (W, x) be a solution to the \mathcal{BP}_ϵ . This point is also an ϵ -accurate Pareto stationarity point for $\{l_i(x)\}$ satisfying*

$$\min_{w \in \mathcal{W}} \|G(x)w\|^2 = \mathcal{O}(\epsilon).$$

Table 9: Additional results on Cityscapes (2-task) dataset with different λ values.

METHOD	SEGMENTATION		DEPTH		$\Delta m\% \downarrow$
	MIOU \uparrow	PIX ACC \uparrow	ABS ERR \downarrow	REL ERR \downarrow	
STL	74.01	93.16	0.0125	27.77	
FAIRGRAD (BAN & JI, 2024)	75.72	93.68	0.0134	32.25	5.18
LDC-MTL ($\tau = 1, \lambda = 0.02$)	73.18	92.78	0.0124	29.67	1.96 ± 1.25
LDC-MTL ($\tau = 1, \lambda = 0.05$)	74.50	93.40	0.0124	28.99	0.79 ± 1.10
LDC-MTL ($\tau = 1, \lambda = 0.06$)	74.84	93.43	0.0123	29.61	0.92 ± 0.95
LDC-MTL ($\tau = 1, \lambda = 0.07$)	75.40	93.42	0.0125	29.25	0.88 ± 1.01
LDC-MTL ($\tau = 1, \lambda = 0.08$)	75.34	93.35	0.0127	29.70	1.64 ± 1.04
LDC-MTL ($\tau = 1, \lambda = 0.09$)	74.97	93.50	0.0123	28.90	0.18 ± 0.96
LDC-MTL ($\tau = 1, \lambda = 0.1$)	74.53	93.42	0.0128	26.79	-0.57 ± 1.17

Table 10: Additional results on Cityscapes (2-task) dataset with different weights of LS.

METHOD	SEGMENTATION		DEPTH		$\Delta m\% \downarrow$
	MIOU \uparrow	PIX ACC \uparrow	ABS ERR \downarrow	REL ERR \downarrow	
STL	74.01	93.16	0.0125	27.77	
LDC-MTL ($\tau = 1, \lambda = 0.1$)	74.53	93.42	0.0128	26.79	-0.57 ± 1.17
LS ($w_1 = 0.1, w_2 = 0.9$)	74.00	92.92	0.0144	29.23	5.13 ± 1.10
LS ($w_1 = 0.2, w_2 = 0.8$)	75.09	93.58	0.0136	33.73	7.18 ± 0.99
LS ($w_1 = 0.3, w_2 = 0.7$)	74.10	93.08	0.0153	35.38	12.38 ± 1.78
LS ($w_1 = 0.4, w_2 = 0.6$)	74.95	93.43	0.0175	43.15	23.47 ± 1.77
LS ($w_1 = 0.6, w_2 = 0.4$)	74.48	93.39	0.0186	43.93	26.53 ± 1.77
LS ($w_1 = 0.8, w_2 = 0.2$)	74.24	93.15	0.0192	61.24	43.19 ± 6.50

Table 11: Additional result on the loss orders with CelebA.

Dataset	$\Delta m\%$
CelebA	-1.31 ± 0.26
CelebA(reorder)	-1.28 ± 0.23

Proof. According to the definition of \mathcal{BP}_ϵ , its solution (W, x) satisfies that

$$g(W, x) - g(W, x^*) \leq \epsilon. \quad (7)$$

Further, according to Assumption 1, we can obtain

$$g(W, x) \geq g(W, x^*) + \nabla_x g(W, x^*)(x - x^*) + \frac{1}{2L_g} \|\nabla_x g(W, x) - \nabla_x g(W, x^*)\|^2.$$

Since $x^* \in \arg \min_x g(W, x)$ and $g(W, x) = \sum_{i=1}^K \sigma_i(W) \tilde{l}_i(x)$, we have $\nabla_x g(W, x^*) = 0$ and $\nabla_x g(W, x) = \sum_{i=1}^K \sigma_i(W) \nabla_x \tilde{l}_i(x) = \tilde{G}(x) \sigma(W)$. We can obtain,

$$\|\tilde{G}(x) \sigma(W)\|^2 \leq 2L_g(g(W, x) - g(W, x^*)) = \mathcal{O}(\epsilon), \quad (8)$$

where the last inequality follows from Equation (7). Furthermore, since we have used softmax at the last layer of our neural network, $\sigma(W)$ belongs to the probability simplex \mathcal{W} . Thus, we can derive

$$\min_{w \in \mathcal{W}} \|\tilde{G}(x) w\|^2 \leq \|\tilde{G}(x) \sigma(W)\|^2 = \mathcal{O}(\epsilon).$$

Thus, the solution (W, x) to the \mathcal{BP}_ϵ also satisfies Pareto stationarity of the normalized loss functions $\{\tilde{l}_i\}$. Then we show the equivalence between the Pareto stationarities for the original loss functions $\{l_i\}$ and the normalized loss functions $\{\tilde{l}_i\}$. First, if there is no normalization, the above eq. (8) naturally recovers

$$\min_{w \in \mathcal{W}} \|G(x) w\|^2 = \min_{w \in \mathcal{W}} \|\tilde{G}(x) w\|^2 \leq \|\tilde{G}(x) \sigma(W)\|^2 = \mathcal{O}(\epsilon).$$

Then, for the rescaled normalization, $\tilde{l}_i(x) = \frac{l_i(x)}{l'_i}$ where $\forall i, l'_i = \mathcal{O}(1)$. Thus, we can have

$$\min_{w \in \mathcal{W}} \|G(x) w\|^2 \leq \|G(x) \sigma(W)\|^2 \leq L_{\max}^2 \|\tilde{G}(x) \sigma(W)\|^2 = \mathcal{O}(\epsilon),$$

where $L_{\max} = \max_i l'_i$. Finally, for the logarithmic normalization, $\tilde{l}_i(x) = \log \left(\frac{l_i(x)}{l_{i,0}} \right) = \lim_{\kappa \rightarrow 1} \frac{\left(\frac{l_i(x)}{l_{i,0}} \right)^{1-\kappa} - 1}{1-\kappa}$.

Furthermore, according to the Proposition 6.1 in Ban & Ji 2024, the Pareto front of the $(\tilde{l}_1(x), \tilde{l}_2(x), \dots, \tilde{l}_K(x))$ which can be considered as κ -fair functions is the same as that of loss functions $\left(\frac{l_1(x)}{l_{1,0}}, \frac{l_2(x)}{l_{2,0}}, \dots, \frac{l_K(x)}{l_{K,0}} \right)$. Therefore, for an ϵ -accurate Pareto stationarity point x of the normalized loss functions, we can obtain

$$\min_{w \in \mathcal{W}} \|G'(x) w\|^2 = \mathcal{O}(\epsilon),$$

where $G'(x) = \left(\frac{\nabla l_1(x)}{l_{1,0}}, \frac{\nabla l_2(x)}{l_{2,0}}, \dots, \frac{\nabla l_K(x)}{l_{K,0}} \right)$. Furthermore, we can obtain

$$\min_{w \in \mathcal{W}} \|G(x) w\|^2 \leq \min_{w \in \mathcal{W}} (L'_{\max})^2 \|G'(x) w\|^2 = \mathcal{O}(\epsilon),$$

where $L'_{\max} = \max_i l_{i,0} = \mathcal{O}(1)$. Then, with our normalization approaches, there is an equivalence between the Pareto stationarities of the original loss functions $\{l_i\}$ and the normalized loss functions $\{\tilde{l}_i\}$. The proof is complete. \square

Theorem 2 (Restatement of Theorem 1). *Suppose Assumptions 1-2 are satisfied. Select hyperparameters*

$$\alpha \in (0, \frac{1}{L_f + \lambda(2L_g + L_g^2 \mu)}], \beta \in (0, \frac{1}{L_g}], \lambda = L \sqrt{3\mu\epsilon^{-1}}, \text{ and } N = \Omega(\log(\alpha t)).$$

(i) *Our method with the updates eq. (3) and eq. (4) (i.e., Algorithm 2 in the appendix) finds an ϵ -accurate stationary point of the problem \mathcal{BP}_λ . If this stationary point is a local/global solution to \mathcal{BP}_λ , it is also a local/global solution to \mathcal{BP}_ϵ . Furthermore, it is also an ϵ -accurate Pareto stationary point for loss functions $l_i(x), i = 1, \dots, K$.*

(ii) *Moreover, if $\|\nabla_W g(W^t, z_N^t)\| = \mathcal{O}(\epsilon)$ for $t = 1, \dots, T$. The simplified method in Algorithm 1 also achieves the same convergence guarantee as that in (i).*

Proof. We start with the first half of our theorem. Directly from Theorem 3 in Shen & Chen 2023, Algorithm 2 achieves an ϵ -accurate stationary point of \mathcal{BP}_λ with $\tilde{\mathcal{O}}(\epsilon^{-1.5})$ iterations such that

$$\frac{1}{T} \sum_{t=0}^{T-1} \|\nabla f(W^t, x^t) + \lambda(\nabla g(W^t, x^t) - \nabla g(W^t, x_t^*))\|^2 \leq \frac{F(W^0, x^0)}{\alpha T} + \frac{10L^2L_g^2}{T} = \mathcal{O}(\epsilon).$$

Recall that $F(W^0, x^0) = f(W^0, x^0) + \lambda(g(W^0, x^0) - g(W^0, x_0^*))$. According to the Proposition 2 in Shen & Chen 2023 by setting $\delta = \epsilon$ therein, we can have $g(W^T, x^T) - g(W^T, x_T^*) \leq \epsilon$ if this stationary point is local/global solution to \mathcal{BP}_λ . Then by using Lemma 1, we know that this ϵ -accurate stationary point is also an ϵ -accurate Pareto stationary point of normalized functions $\{\tilde{l}_i(x)\}$ satisfying

$$\min_{w \in \mathcal{W}} \|G(x^T)w\|^2 = \mathcal{O}(\epsilon).$$

The proof of the first half of our theorem is complete.

Then, for the second half, since we have built the connection between the stationarity of \mathcal{BP}_λ and Pareto stationarity, we prove that the single-loop Algorithm 1 achieves an ϵ -accurate stationary point of \mathcal{BP}_λ . Recall that

$$\begin{aligned} & \|\nabla f(W^t, x^t) + \lambda(\nabla g(W^t, x^t) - \nabla g(W^t, x_t^*))\|^2 \\ & \stackrel{(i)}{\leq} 2\|\nabla f(W^t, x^t) + \lambda\nabla g(W^t, x^t)\|^2 + 2\lambda^2\|\nabla g(W^t, x_t^*)\|^2 \\ & \stackrel{(ii)}{=} 2\|\nabla f(W^t, x^t) + \lambda\nabla g(W^t, x^t)\|^2 + 2\lambda^2\|\nabla_W g(W^t, x_t^*)\|^2 \\ & \stackrel{(iii)}{\leq} 2\|\nabla f(W^t, x^t) + \lambda\nabla g(W^t, x^t)\|^2 + 4\lambda^2\|\nabla_W g(W^t, x_t^*) - \nabla_W g(W^t, z_N^t)\|^2 \\ & \quad + 4\lambda^2\|\nabla_W g(W^t, z_N^t)\|^2, \end{aligned} \tag{9}$$

where (i) and (iii) both follow from Young's inequality, and (ii) follows from $\nabla_x g(W^t, x_t^*) = 0$. Besides, recall that z_N^t is the intermediate output of the subloop in Algorithm 2. We next provide the upper bounds of the above three terms on the right-hand side (RHS). For the first term, we utilize the smoothness of $\Phi(\theta^t) = \nabla f(\theta^t) + \lambda\nabla g(\theta^t)$ where $L_\Phi = L_f + \lambda L_g$ and $\theta^t = (W^t, x^t)$.

$$\begin{aligned} \Phi(\theta^{t+1}) & \leq \Phi(\theta^t) + \langle \nabla \Phi(\theta^t), \theta^{t+1} - \theta^t \rangle + \frac{L_\Phi}{2} \|\theta^{t+1} - \theta^t\|^2 \\ & \stackrel{(i)}{\leq} \Phi(\theta^t) - \frac{\alpha}{2} \|\nabla \Phi(\theta^t)\|^2, \end{aligned}$$

where (i) follows from $\alpha \leq \frac{1}{L_\Phi} = \mathcal{O}(\lambda^{-1})$. Thus, we can obtain

$$\|\nabla \Phi(\theta^t)\|^2 \leq \frac{2}{\alpha} (\Phi(\theta^t) - \Phi(\theta^{t+1})). \tag{10}$$

Then for the second term on the RHS in eq. (9), we follow the same step in the proof of Theorem 3 in Shen &

Chen 2023 and obtain

$$\begin{aligned}
& 4\lambda^2 \|\nabla_W g(W^t, x_t^*) - \nabla_W g(W^t, z_N^t)\|^2 \\
& \leq 4\lambda^2 L_g^2 \mu \left(1 - \frac{\beta}{2\mu}\right)^N (g(W^t, x^t) - g(W^t, x_t^*)) \\
& \stackrel{(i)}{\leq} 4\lambda^2 L_g^2 \left(1 - \frac{\beta}{2\mu}\right)^N \|\nabla_x g(W^t, x^t)\|^2 \\
& = 4\lambda^2 L_g^2 \left(1 - \frac{\beta}{2\mu}\right)^N \left\| \frac{x^{t+1} - x^t + \alpha \nabla_x f(W^t, x^t)}{\alpha \lambda} \right\|^2 \\
& \stackrel{(ii)}{\leq} 8\lambda^2 L_g^2 \left(1 - \frac{\beta}{2\mu}\right)^N \left(\frac{\|\theta^{t+1} - \theta^t\|^2}{\alpha^2 \lambda^2} + \frac{L^2}{\lambda^2} \right) \\
& \stackrel{(iii)}{\leq} \frac{1}{2\alpha^2} \|\theta^{t+1} - \theta^t\|^2 + \frac{2L^2 L_g^2}{\alpha^2 t^2} \\
& = \frac{1}{2} \|\nabla \Phi(\theta^t)\|^2 + \frac{2L^2 L_g^2}{\alpha^2 t^2},
\end{aligned} \tag{11}$$

where (i) follows from the PL condition, (ii) follows from Young's inequality and Assumption 1, and (iii) follows from the selection on $N \geq \max\{-\log_{c_\beta}(16L_g^2), -2\log_{c_\beta}(2\alpha t)\}$ with $c_\beta = 1 - \frac{\beta}{2\mu}$. Lastly, for the last term at the RHS in eq. (9), we have,

$$4\lambda^2 \|\nabla_W g(W^t, z_N^t)\|^2 = \mathcal{O}(\lambda^2 \epsilon^2), \tag{12}$$

where this inequality follows from our experimental observation. Furthermore, substituting eq. (10), and eq. (11) into eq. (9) yields

$$\begin{aligned}
& \|\nabla f(W^t, x^t) + \lambda(\nabla g(W^t, x^t) - \nabla g(W^t, x_t^*))\|^2 \\
& \leq \frac{5}{2} \|\nabla \Phi(\theta^t)\|^2 + \frac{2L^2 L_g^2}{\alpha^2 t^2} + 4\lambda^2 \|\nabla_W g(W^t, z_N^t)\|^2 \\
& \leq \frac{5}{\alpha} (\Phi(\theta^t) - \Phi(\theta^{t+1})) + \frac{2L^2 L_g^2}{\alpha^2 t^2} + 4\lambda^2 \|\nabla_W g(W^t, z_N^t)\|^2.
\end{aligned} \tag{13}$$

Therefore, telescoping the above inequality yields,

$$\begin{aligned}
& \frac{1}{T} \sum_{t=0}^{T-1} \|\nabla f(W^t, x^t) + \lambda(\nabla g(W^t, x^t) - \nabla g(W^t, x_t^*))\|^2 \\
& = \mathcal{O}\left(\frac{\lambda}{\alpha T} + \frac{1}{\alpha^2 T} + \lambda^2 \epsilon^2\right).
\end{aligned}$$

According to the parameter selection that $\lambda = \mathcal{O}(\epsilon^{-\frac{1}{2}})$, $\alpha = \mathcal{O}(\epsilon^{\frac{1}{2}})$, and $T = \mathcal{O}(\epsilon^{-2})$, we can obtain

$$\frac{1}{T} \sum_{t=0}^{T-1} \|\nabla f(W^t, x^t) + \lambda(\nabla g(W^t, x^t) - \nabla g(W^t, x_t^*))\|^2 = \mathcal{O}(\epsilon).$$

Therefore, Algorithm 1 can achieve a stationary point of \mathcal{BP}_λ with $\mathcal{O}(\epsilon^{-2})$ iterations. If this stationary point is a local/global solution to \mathcal{BP}_λ , it is also a solution to \mathcal{BP}_ϵ according to Proposition 2 in Shen & Chen 2023. Then by using Lemma 1, we know this stationary point is also an ϵ -accurate Pareto stationary point of the original loss functions. The proof is complete. \square